Taylor & Francis
Taylor & Francis Group

Journal of Information Display

ISSN: 1598-0316 (Print) 2158-1606 (Online) Journal homepage: www.tandfonline.com/journals/tjid20

Photo response of a-IGZO thin films as a function of annealing temperature

Seung Jae Moon, Ju-Yeon Kim, Junghwan Kim & Byung Seong Bae

To cite this article: Seung Jae Moon, Ju-Yeon Kim, Junghwan Kim & Byung Seong Bae (12 Aug 2025): Photo response of a-IGZO thin films as a function of annealing temperature, Journal of Information Display, DOI: 10.1080/15980316.2025.2541731

To link to this article: https://doi.org/10.1080/15980316.2025.2541731

© 2025 The Author(s). Published by Informa UK Limited, trading as Taylor & Francis Group on behalf of the Korean Information Display Society

Published online: 12 Aug 2025.

Submit your article to this journal

Article views: 197

View related articles

View Crossmark data

Full Terms & Conditions of access and use can be found at
https://www.tandfonline.com/action/journalInformation?journalCode=tjid20

JOURNAL OF INFORMATION DISPLAY
https://doi.org/10.1080/15980316.2025.2541731

Taylor & Francis
Taylor & Francis Group

OPEN ACCESS Check for updates

Photo response of a-IGZO thin films as a function of annealing temperature

Seung Jae Moon[a,b], Ju-Yeon Kim[c], Junghwan Kim[b] and Byung Seong Bae[a]

[a]Department of Semiconductor Engineering, Hoseo University, Asan-City, Korea; [b]Graduate School of Semiconductor Materials and Devices Engineering, Ulsan National Institute of Science and Technology (UNIST), Ulsan, South Korea; [c]Lam Research Co, Korea Technology Center, Yongin-si, Rep. of Korea

ABSTRACT

This paper investigated the photo response behavior of amorphous indium gallium zinc oxide (a-IGZO) thin films, identifying three distinct photoconductivity types corresponding to different oxygen vacancy concentrations: Type I (low vacancy density), Type II (intermediate density), and Type III (high vacancy density). The results reveal that the photoconductive properties of a-IGZO are massively influenced by oxygen vacancy concentration, which can be precisely controlled through vacuum annealing. Type I films exhibit rapid recombination of photogenerated electron–hole pairs when illumination is removed, suggesting minimal involvement of defect states. Contrarily, Types II and III yield slower photo response and increasingly persistent photoconductivity, reflecting the growing presence of ionized oxygen vacancies that act as donor states. This demonstrates the essential impact of vacancy-induced defect levels on carrier trapping and recombination behavior. In films with low vacancy densities, defect generation under illumination was observable, while in films with higher vacancy concentrations, incident light ionizes oxygen vacancies, increasing donor state density and enhancing photoconductivity. Moreover, the observed photo response characteristics provide a useful indicator of film quality. The study's findings emphasize the role of oxygen vacancy in the electronic and optoelectronic properties of a-IGZO, offering practical guidance for implementing quality IGZO films.

ARTICLE HISTORY
Received 12 December 2024
Accepted 17 July 2025

KEYWORDS
IGZO; photoconductivity; vacancy; trap states

1. Introduction

Amorphous oxide semiconductor (AOS) thin-film transistors (TFTs) have attracted considerable attention due to their various advantages [1–13], such as higher mobility compared to amorphous silicon (a-Si) TFTs, simpler fabrication processes than low-temperature polycrystalline silicon (LTPS) TFTs, and optical transparency resulting from their wide bandgap [14–17]. These characteristics underscore AOS TFTs as promising candidates for next-generation switching devices in large-area, high-resolution, and transparent displays.

However, stability issues – particularly those associated with oxygen vacancies – remain a pressing challenge for oxide TFTs [18,19]. Oxygen vacancies are commonly regarded as the primary source of instability and the dominant intrinsic defect in materials [17,20–23]. Therefore, to enhance device reliability, it is essential to minimize oxygen vacancies and control the incorporation of hydrogen and water [24–26]. Reducing hydrogen and water content, along with suppressing oxygen vacancy formation, is critical for improving long-term stability [27,28].

Previous studies have examined the stability of amorphous IGZO (a-IGZO) TFTs under various stress conditions, such as illumination stress (IS), negative bias stress (NBS), negative bias illumination stress (NBIS), and persistent photoconductivity (PPC) in oxide films [5,7,29]. However, the complexity of the TFT structure brings about challenges for analyzing stability mechanisms. Thus, using a single a-IGZO film allows for a more straightforward investigation of its intrinsic stability.

Unlike hydrogenated amorphous silicon, which exhibits a sharp rise in photocurrent under illumination and a rapid decay once the light is turned off – primarily due to electron–hole pair generation and recombination [30] – a-IGZO films demonstrate a gradual increase in photoconductivity during light exposure and a slow decay in the dark, a behavior characteristic of persistent photoconductivity (PPC) [8,16].

Accordingly, this study observed and analyzed abrupt increases and decreases in the photoresponse of a-IGZO thin films. Various photoconductivity behaviors were identified, and three distinct types of photoconduction were revealed and thoroughly investigated. These

CONTACT Byung Seong Bae bsbae3@hoseo.edu Department of Semiconductor Engineering, Hoseo University, Asan-City, Chungnam 31499, Rep. of Korea

ISSN (print): 1598-0316; ISSN (online): 2158-1606
© 2025 The Author(s). Published by Informa UK Limited, trading as Taylor & Francis Group on behalf of the Korean Information Display Society
This is an Open Access article distributed under the terms of the Creative Commons Attribution License (http://creativecommons.org/licenses/by/4.0/), which permits unrestricted use, distribution, and reproduction in any medium, provided the original work is properly cited. The terms on which this article has been published allow the posting of the Accepted Manuscript in a repository by the author(s) or with their consent.

phenomena were further examined by studying the annealing-dependent photoresponse of the films.

2. Experimental

An a-IGZO thin films were deposited on glass by sputtering under a 0.3 Pa Ar and 0.5 Pa O_2 flow at a substrate temperature of 100 °C. The Al electrodes were formed by thermal evaporation through a shadow mask. Before metal deposition, the deposited a-IGZO films were annealed at various temperatures, such as 150°C, 200°C, 250°C, 300°C, and 400°C. The thicknesses of the a-IGZO thin films and Al electrodes were 150 and 100 nm, respectively. The Al electrodes were 1,500 µm wide and 100 µm long, and the Ohmic contact was confirmed by measurement of current–voltage characteristics. The photocurrent of a-IGZO thin films under light illumination with various wavelengths was monitored. To avoid the effects of several factors such as moisture, light, and other impurities, all the measurements were carried out in a dark vacuum chamber with a measurement temperature of 60°C. The photocurrent of the a-IGZO thin film was measured using 400, 470, 530, and 850 nm LEDs. The photon fluxes of the LEDs were fixed to 1.83×10^{17} photons/cm^2·s. The photocurrents were monitored during 1 hour of illumination, and the dark currents were monitored for 1 hour after turning off the illumination.

3. Results and discussion

Figure 1 shows the photo-response of an as-deposited a-IGZO film under 400 nm LED illumination. After 1 hour of light exposure, the light was turned off for 200 s before re-illumination. During the initial illumination, the photoconductivity exhibited a sharp rise, followed by a rapid decline, eventually stabilizing at a constant level. Upon light off, the photoconductivity quickly dropped to dark conductivity. When the light was turned on again, the photoconductivity increased to the same saturated level as the first illumination, but without the initial sharp increase and subsequent rapid decrease.

Because the surface is sensitive to light illumination, the surface effect should be considered during the first light illumination. The oxygen adsorbed on the a-IGZO layer forms a depletion layer at the surface [31–33]. Therefore, the photo-generated electrons were depleted from the surface defects, resulting in large photo-conduction because of the low recombination rate at the surface. As the oxygen desorbed under light exposure [31], the recombination rate increased, rapidly decreasing photoconductivity. This oxygen desorption was completed by the second illumination, explaining the lack of a large increase in conductivity during the second light exposure.

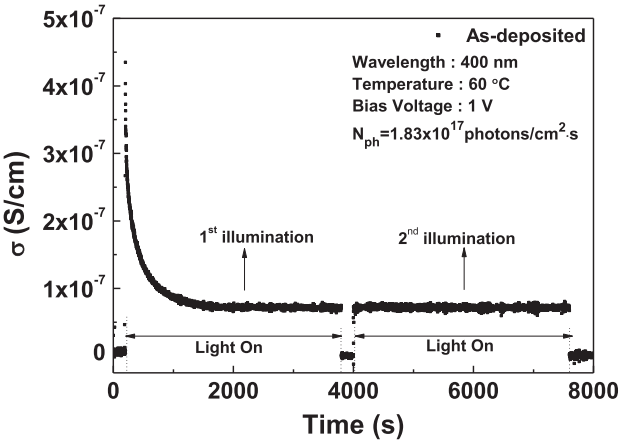

Figure 1. Photo-response of as-deposited a-IGZO shows an initial rapid decrease in photoconductivity followed by saturation. When the light is turned off, the conductivity decreases quickly to a dark conductivity, which increases rapidly again when the light is turned on.

Figure 1 represents a low dark conductivity of approximately 10^{-7} S/cm, indicating low self-doping. The low concentration of oxygen vacancies, which are closely associated with self-doping, contributes to this observed dark conductivity. This low vacancy concentration also accounts for the rapid changes in conductivity when the illumination is switched on and off.

Figure 2(a, b) describe the photoconductivity after annealing at temperatures of 150°C, 200°C, and 250°C. At 150 and 200°C, the photoconductivity decreased during illumination and rapidly returned to the dark conductivity once the light was turned off. The gradual decline in photoconductivity during illumination can be related to an increase in the recombination rate, reflecting the balance between the rate of recombination and generation. As the recombination rate increased, the excess electrons generated by light absorption were diminished. While the exact cause of the increased recombination rate is not fully understood, the presence of additional trap states likely contributes [34–37]. Immediately after illumination ceased, the photo-generated electrons rapidly disappeared due to electron–hole recombination, as depicted in Figure 2(a, b).

After annealing at 250°C, the photoconductivity of the a-IGZO film increased under light illumination, followed by persistent photoconductivity (PPC) after an initial rapid decrease in photoconductivity when the light was turned off. Reduced trap states enhance photoconductivity by lowering the recombination rate of photogenerated charge carriers. However, light illumination typically increases trap states, making the possibility of reduced

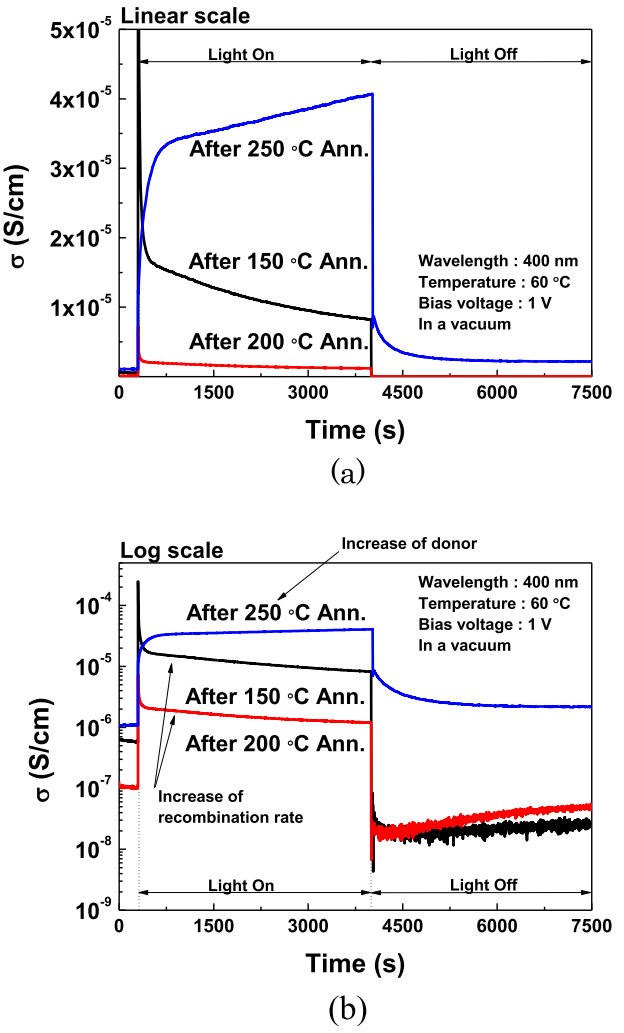

Figure 2. Comparison of the photo – and dark-relaxation of the conductivities for various annealing temperatures (150°C, 200°C, and 250°C), (a) linear scale and (b) log scale.

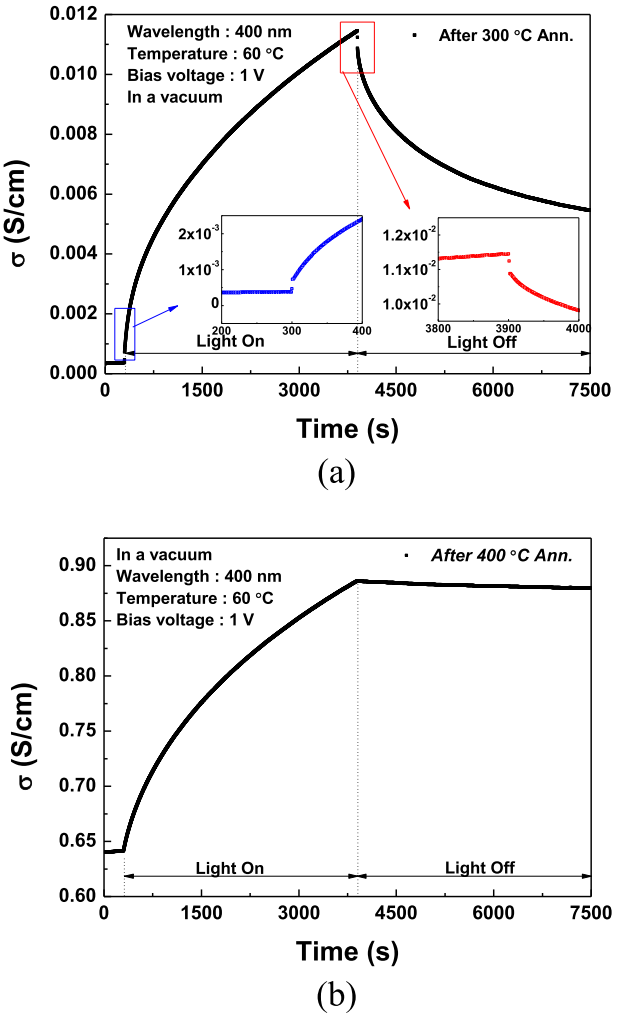

Figure 3. Photo-response according to the annealing temperatures of (a) 300°C and (b) 400°C.

trap states unlikely. Instead, the gradual increase in photoconductivity can be attributed to self-doping effects caused by the ionization of oxygen vacancies. When exposed to light, oxygen vacancies in the a-IGZO film release electrons, transitioning to ionized states. These free electrons contribute to the conduction band, enhancing conductivity. This self-doping process is a cumulative effect, as prolonged illumination can progressively ionize more vacancies, gradually increasing the overall photoconductivity. [26] While the excess electrons excited from the valence band rapidly recombine or dissipate after the light is turned off, the gradual decrease in photoconductivity is associated with the slow neutralization of donor states, primarily ionized oxygen vacancies. These ionized oxygen vacancies act as donor sites by releasing free electrons during illumination. Once the light is turned off, the recombination process between the ionized oxygen vacancies and ambient oxygen or other charge-trapping mechanisms occurs gradually. This reduces the effective number of donor states over time, even leading to a slower decline in photoconductivity compared to the rapid disappearance of excited valence-band electrons.

Figure 3(a, b) show the photo response after annealing at 300°C and 400°C. At these higher annealing temperatures, both the photoconductivity and persistent dark conductivity increased. After annealing at 300°C, the photoconductivity of the material revealed a two-phase increase: an initial small but abrupt rise, followed by a gradual and sustained increase. The abrupt rise is mainly attributed to the immediate generation of electron–hole pairs upon light illumination. These pairs are created through band-to-band excitation, where photons with sufficient energy excite electrons from the valence band to the conduction band, resulting in an instant increase in conductivity. The subsequent gradual rise in photoconductivity can be explained by the progressive activation of donor states, such as ionized oxygen vacancies, during

illumination. When the light was turned off, the conductivity exhibited an initial rapid decrease, followed by a slower decline over time. The sharp drop in conductivity can be linked to the immediate recombination of photogenerated electron–hole pairs, which were excited during light exposure through band-to-band transitions. This process occurs rapidly as the photogenerated carriers recombine, either through direct electron–hole recombination or by being captured by shallow trap states in the material. These traps, often correlated with defects or impurities, can temporarily capture charge carriers, decreasing their contribution to conductivity. The fast decay is driven by the short-lived nature of these electron–hole pairs and the capture of carriers by these low-energy states, leading to a quick reduction in conductivity. In contrast, the slower, gradual decrease in conductivity is linked to the dynamics of donor states, such as ionized oxygen vacancies. These states, activated under illumination, slowly neutralize as oxygen or other ambient species interact with the material, recombining free electrons with these donor sites. The slower rate reflects the more gradual kinetics of these reactions compared to the faster band-to-band recombination. This dual-phase behavior highlights the interplay between transient charge carrier dynamics and the structural or chemical changes within the material.

At an annealing temperature of 400°C, no rapid change in conductivity was observed, as the self-doped electron density significantly exceeded the photogenerated electron density. The rapid conductivity change, typically induced by band-to-band transitions from incident photons, remained unaffected by the annealing process. On the other hand, the slow increase and decrease in conductivity were attributed to the ionization of oxygen vacancies, a relatively slow process. Ionized oxygen vacancies act as donor defects, increasing the electron density. Consequently, the higher annealing temperature increased the number of vacancies, enhancing the donor states and renders the effects of band-to-band transitions negligible compared to the donor state contributions.

Although the photo-responses varied with annealing temperature, X-ray diffraction (XRD) analysis confirmed that all samples remained amorphous without significant structural changes. The measured bandgap increased with higher annealing temperatures, attributable to the higher concentration of oxygen vacancies.

Figure 4 differentiates the change in dark conductivity at various annealing temperatures. The dark conductivity increased with higher annealing temperatures, consistent with previous studies. This change in conductivity is mostly attributed to donor levels created by oxygen deficiencies, particularly through the formation of oxygen

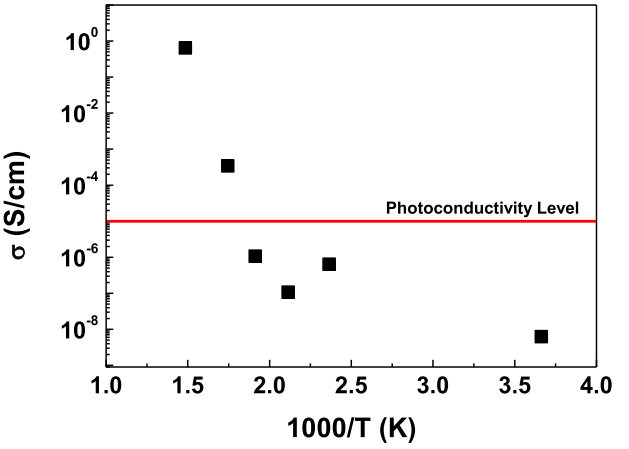

Figure 4. Dark conductivities of the a-IGZO film at various annealing temperatures.

vacancies. During high-temperature annealing, oxygen atoms are expelled from the material, reducing the overall oxygen content. Then, this reduction results in the creation of doubly ionized oxygen vacancies (V_O^{2+}), which serve as donor states in the a-IGZO film. These donor states contribute free electrons to the conduction band, increasing the dark conductivity. As the annealing temperature increases, the number of oxygen vacancies also rises, making doubly ionized oxygen vacancies more prevalent. This enhanced presence of donor levels is directly responsible for the observed increase in conductivity, as the available free carriers improve the overall electrical conductivity of the material [38].

At lower annealing temperatures, the photocurrent is mainly generated by electron–hole pair (e-h pair) generation through band-to-band excitation, as shown in Figure 2(a). This indicates that the photoconductivity due to e-h pair generation is approximately 10^{-5} S/cm, as illustrated in Figure 4 and Figure 5. The photoconductivity from band-to-band electron excitation remained relatively constant regardless of the annealing temperature. However, the dark conductivity increased with higher annealing temperatures due to a greater number of oxygen vacancies, which act as donors when doubly ionized.

In the as-fabricated sample, photocurrent decreased during light illumination, likely due to an increased recombination rate. Additionally, dark conductivity was significantly lower than the photoconductivity, as indicated on the left side of Figure 5, due to the low concentration of oxygen vacancies, resulting in minimal self-doping by doubly ionized oxygen vacancies.

For the sample annealed at 300°C, dark conductivity increased due to self-doping from the higher concentration of oxygen vacancies. However, dark conductivity remained lower than the photoconductivity induced by

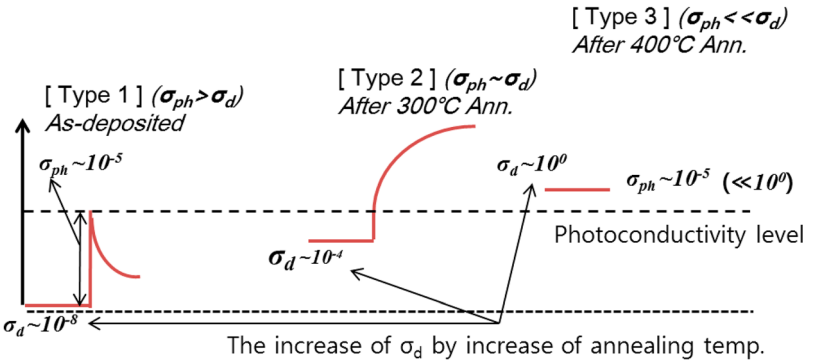

Figure 5. Schematic diagram of the photo responses at various annealing temperatures.

e-h pair generation. Consequently, a slow increase in conductivity followed a small, abrupt rise in photoconductivity.

At 400°C, the level of self-doping increased significantly due to the higher concentration of oxygen vacancies induced by high-temperature annealing. As a result, dark conductivity exceeded photoconductivity from e-h pair generation. Because dark conductivity was substantially higher than photoconductivity, no sudden increase in conductivity was observed during light illumination. Instead, a slow increase in conductivity, corresponding to the growing number of ionized oxygen vacancies, was observed.

In summary, this research identified three distinct photoconductive behavior types in a-IGZO films, each linked to varying oxygen vacancy densities:

Type I (lower oxygen vacancy): This type has a low oxygen vacancy concentration. In this case, photoconductivity initially increases sharply under light illumination due to band-to-band electron excitation, where electrons are excited from the valence band to the conduction band. However, after the light is turned off, the conductivity decreases quickly, returning to its dark conductivity state. This rapid recovery is chiefly driven by the recombination of the photogenerated electron–hole pairs, as there are fewer ionized oxygen vacancies available to act as donor states, swiftly returning to the dark state. The behavior is largely dominated by band-to-band transitions, as the lower oxygen vacancy density limits the number of available donor levels.

Type II (intermediate oxygen vacancy): This behavior corresponds to an intermediate oxygen vacancy density, where the photoconductivity exhibits a small, abrupt increase followed by a gradual rise during light illumination. The initial sharp increase is attributed to the generation of electron–hole pairs through band-to-band excitation, where photons excite electrons from the valence band to the conduction band. This rapid increase is followed by a more gradual rise in conductivity, which is due to the continuous ionization of oxygen vacancies. As these vacancies become ionized, they contribute free electrons to the conduction band, further enhancing the conductivity over time. Upon turning off the light, the conductivity initially decreases rapidly as the photogenerated electron–hole pairs recombine quickly. However, the decrease then slows down as the ionized oxygen vacancies gradually recombine with ambient oxygen or other species, causing a more gradual reduction in free charge carriers. The slower decline is linked to the neutralization of the donor defects (oxygen vacancies), which act as persistent donor states that contribute to the photoconductivity over time. Thus, the transition between fast and slow changes in conductivity reflects the interplay between transient band-to-band recombination and the more persistent contribution of donor states from oxygen vacancies.

Type III (higher oxygen vacancy): This behavior is associated with a high oxygen vacancy density, where dark conductivity and photoconductivity are increased. In this situation, dark conductivity is high due to the significant number of ionized oxygen vacancies that act as donor states, providing a continuous supply of free electrons to the conduction band. Under light illumination, photoconductivity increases gradually as the photogenerated charge carriers are supplemented by these ionized donor states. When the light is turned off, the relaxation back to dark conductivity occurs more slowly, as the ionized oxygen vacancies remain as active donor states, continuously contributing electrons to the conduction band even after the external light source is removed. This results in a slower decay of photoconductivity.

At higher annealing temperatures, dark and photoconductivity further increase due to a higher oxygen vacancy concentration. The ionized oxygen vacancies dominate the photoconductive response through a self-doping effect, where the vacancies themselves contribute free electrons to the conduction band, overshadowing the contribution from band-to-band transitions.

This self-doping mechanism is more pronounced as the vacancy concentration increases, leading to a more gradual and persistent enhancement in conductivity.

The schematic representation provided thus far requires refinement to more accurately reflect the photoconductivity levels, which vary with oxygen vacancy density. A more precise description, grounded in the underlying conduction mechanisms, is necessary to enhance understanding of the observed behavior.

Dark conductivity σ_d is directly proportional to the carrier density and mobility, as well as the elementary charge of the carrier. The carrier density in IGZO film is influenced by various factors, including oxygen vacancies, intrinsic defects, the band gap energy, which is determined by process conditions, and the elemental composition ratio, such as that of In, Ga, and Zn. Given that only one sample was used in this experiment, process condition variability is not regarded as a major factor impacting the results. Annealing IGZO (In-Ga-Zn-O) films under vacuum conditions significantly enhances their conductivity by promoting oxygen diffusion out of the material. This process increases oxygen vacancy concentration, which acts as an electron donor by releasing free carriers into the lattice. As IGZO is intrinsically an N-type semiconductor, the majority carriers are electrons, while hole contributions to conductivity are negligible due to their extremely low mobility and density in such systems. Consequently, the elevated electron concentration from oxygen vacancies directly governs the overall electrical conductivity of the annealed IGZO film.

In amorphous indium gallium zinc oxide (a-IGZO) thin films, the total electron carrier density arises from two primary mechanisms: (1) intrinsic thermal excitation of electrons across the bandgap and (2) extrinsic electron donation through the ionization of oxygen vacancies ($V_O{}^{2+}$), which act as shallow donors within the oxide matrix.

The thermally generated electron density through the bandgap, n_T, can be expressed as

$$n_T = G\tau_o \tag{1}$$

where G is the thermal generation rate of electron–hole pairs across the band gap, and τ_o is the carrier lifetime corresponding to the initial concentration of oxygen vacancies N_{V_0}. Given that only one sample was utilized in this experiment, process condition variability is not regarded as a major factor impacting the results.

In the dark state, neutral oxygen vacancies can thermally activate and act as electron donors, contributing to the free electron density. Based on this, the electron density generated by oxygen vacancies, n_V, can be expressed as

$$n_V = \alpha N_{V_0} \tau_o \tag{2}$$

where N_{V_0} is the concentration of neutral oxygen vacancies, and α is the thermal activation coefficient for electron generation, and τ_o is the lifetime of the electron. Accordingly, the total electron carrier density in the dark is

$$n = G\tau_o + \alpha N_{V_0}\tau_o = n_T + \alpha N_{V_0}\tau_o \tag{3}$$

where $n_T = G\tau_o$ corresponds to the intrinsic electron density generated via band-to-band excitation, and $\alpha N_{V_0}\tau_o$ represents the vacancy-induced contribution. The resulting dark conductivity, σ_d, is then given by

$$\sigma_d = ne\mu = G\tau_o\, e\mu + \alpha N_{V_0}\tau_o\, e\mu \tag{4}$$

Since the electrons originating from oxygen vacancies also undergo recombination processes – that is, they are transiently mobile carriers rather than permanently ionized – we assume the same carrier lifetime τ_o applies to thermally generated and vacancy-induced electrons. This expression can be reformulated as

$$\sigma_d = G\tau_o\, e\mu + \tau_o\, e\mu\alpha N_{V_0} = \sigma_{d0}\left(1 + \frac{\alpha N_{Vo}}{G}\right) \tag{5}$$

Here, $\sigma_{do} = G\tau_o e\mu$ represents the baseline conductivity arising from band-to-band carrier generation. This formulation points out the additive effect of defect-related carriers, which becomes particularly significant when the density of oxygen vacancies is high compared to the band-to-band carrier generation.

Considering the band gap energy of $\sim$3.2 eV, effective density of state $\sim 10^{18} \sim 10^{19}/\mathrm{cm}^3$, Eq. (5) indicates that dark conductivity increases with the number of oxygen vacancies, consistent with the recorded enhancement in dark conductivity as the vacuum annealing temperature rises, as illustrated in Figures 2 and 3. Increasing the annealing temperature leads to a rise in oxygen vacancies, which enhances dark conductivity, as specified in the equation. The dark conductivity increased from less than $1 \times 10^{-7} S/\mathrm{cm}$ to $0.64 S/\mathrm{cm}$ as the vacuum annealing temperature was elevated to 400°C. This suggests a significant increase in oxygen vacancies with higher annealing temperatures..

When the dark conductivity is low due to a reduced density of oxygen vacancies, a degradation in photoconductivity is observed during light illumination. This behavior is analogous to the Staebler-Wronski effect in hydrogenated amorphous silicon (a-Si:H) thin films, where prolonged exposure to light generates metastable defect states [39–41]. These states increase the density

of localized traps, enhancing the recombination rate of photogenerated carriers and resulting in a lower concentration of free electrons in the conduction band. In IGZO, a similar mechanism may be responsible, where light-induced defect formation or carrier trapping – particularly under low oxygen vacancy conditions – suppresses the free carrier density. Notably, unlike persistent photoconductivity often observed in IGZO due to shallow donor states associated with oxygen vacancies, this photoconductivity degradation is at least partially reversible, suggesting the involvement of metastable states or structural relaxation effects rather than permanent defect generation [42].

Under these conditions, the photocurrent increases sharply at the onset of illumination, followed by a rapid decrease in photoconductivity, which then slows down, as illustrated in Figure 2(a, b). Upon photocarrier generation, a rapid initial decrease in photoconductivity is observed, attributable to the trapping of holes at pre-existing deep-level trap states. This is followed by a slower decay phase, which is associated with the progressive reduction in carrier lifetime. The slow decay is usually linked to the formation of metastable defect states or the generation of additional recombination centers under prolonged illumination. These defects promote enhanced non-radiative recombination pathways, thereby reducing carrier lifetime and contributing to the persistent decline in photoconductivity. Consequently, the observed decrease in photocurrent under illumination is primarily attributed to defect formation, rather than to the presence of oxygen vacancies, which exist in relatively low concentrations. These vacancies contribute minimally to donor generation, especially when compared to the substantially larger population of photocarriers generated via band-to-band photoexcitation.

Assuming that oxygen vacancies are the dominant defect species, denoted as N_V, the carrier lifetime before light irradiation, τ_o, can be expressed as:

$$\tau_o = \frac{1}{kN_{Vo}} \tag{6}$$

where N_{V0} represents the initial density of oxygen vacancies before illumination, and k is a proportionality constant defined as the product of the electron capture cross-section and their thermal velocity. The carrier lifetime τ after light exposure is affected by the increase in oxygen vacancy concentration, N_V. As oxygen vacancies act as recombination centers, their increased density leads to a higher recombination rate, thereby reducing the carrier lifetime. This relationship is quantitatively expressed as

$$\tau = \frac{1}{kN_V} \tag{7}$$

If the saturated defect density is denoted by N_∞ and the initial defect density by N_{V0}, the time-dependent defect density can be expressed as

$$N_V(t) = N_{V0} + (N_\infty - N_{V0})\left(1 - \mathrm{e}^{-\frac{t}{\tau_d}}\right) \tag{8}$$

Here, τ_d is the characteristic time constant associated with the generation of light-induced defects. Substituting the time-dependent defect density from Eq. (8) into Eq. (7), the carrier lifetime as a function of time, $\tau(t)$, becomes

$$\tau(t) = \frac{1}{k[N_{V0} + (N\infty - N_{V0})\left(1 - \mathrm{e}^{-\frac{t}{\tau_d}}\right)} \tag{9}$$

Using the initial carrier lifetime $\tau_o = \frac{1}{kN_{Vo}}$ from Eq. (6), Eq. (9) can be rewritten as

$$\tau(t) = \frac{\tau_o}{1 + (N_\infty/N_{V0} - 1)\left(1 - \mathrm{e}^{-\frac{t}{\tau_d}}\right)} \tag{10}$$

Defining a dimensionless constant $\mathrm{A} = N_\infty/N_{V0} - 1$, Eq. (10) simplifies to

$$\tau(t) = \frac{\tau_o}{1 + A\left(1 - \mathrm{e}^{-\frac{t}{\tau_d}}\right)} \tag{11}$$

Under light illumination, band-to-band excitation generates excess carriers with a density of $G_p\tau$, where G_p is the photogeneration rate, and τ is the carrier lifetime. Moreover, electrons excited from gap states – such as oxygen vacancies – contribute to the excess carrier population with a generation rate of $G_{pV}N_V$, where G_{pV} is the photo-generation coefficient associated with oxygen vacancies, and N_V is their concentration. Therefore, the total excess carrier density induced by illumination is the sum of both contributions, that is $G_p\tau + \tau G_{pV}N_V = (G_p + G_{pV}N_V)\tau$.

Therefore, by applying Eq. (10), the photoconductivity σ_p can be expressed as

$$\sigma_p = e\mu(G_p + G_{pV}N_V)\frac{\tau_o}{1 + A\left(1 - \mathrm{e}^{-\frac{t}{\tau_d}}\right)} \tag{11}$$

At $\mathrm{t} = 0$, with $N_V = N_{Vo}$, and can get the initial photoconductivity $\sigma_{po} = e\mu(G_p + G_{pV}N_{Vo})\tau_o$, then Eq. (11) becomes.

$$\sigma_p = \frac{\sigma_{po}}{1 + A\left(1 - \mathrm{e}^{-\frac{t}{\tau_d}}\right)} \tag{12}$$

This behavior indicates a progressive reduction in photoconductivity over time, which is consistent with the

Table 1. Dark conductivity versus initial photoconductivity.

$\sigma_d S/cm$	$\sigma_{po} S/cm$
1.0×10^{-7}	2.0×10^{-6}
6.0×10^{-7}	1.8×10^{-5}
1.0×10^{-6}	1.1×10^{-5}
4.0×10^{-4}	6.0×10^{-4}

Table 2. Dark conductivity versus oxygen vacancies.

$\sigma_d S/cm$	$N_{Vo} cm^{-3}$
1.0×10^{-7}	1.0×10^{15}
6.0×10^{-7}	6.0×10^{15}
1.0×10^{-6}	1.0×10^{16}
4.0×10^{-4}	4.0×10^{18}

trends noted in Figures 2 and 3. The temporal evolution predicted by Eq. (12) aligns well with the experimental data, supporting the proposed model's validity.

Here, σ_{po} denotes the initial photoconductivity measured immediately after the rapid drop following light exposure. The total measured conductivity σ comprises the dark conductivity and the photoconductivity components. Therefore, σ is.

$$\sigma = \sigma_d + \sigma_{po} \frac{1}{1 + A\left(1 - \mathrm{e}^{-\frac{t}{\tau_d}}\right)} \tag{13}$$

Table 1 lists the observed dark conductivities and initial photo conductivities.

By applying curve fitting, a relationship between the initial photo conductivities and the dark conductivities was obtained, as:

$$\sigma_{po} = -5.96 \times 10^{-4} e^{-\frac{\sigma_d}{5.38 \times 10^{-5}}} + 6.0 \times 10^{-4} \tag{14}$$

Upon illumination, excess electron carriers are generated primarily through two mechanisms: band-to-band excitation of electron – hole pairs and photoionization of oxygen vacancies. The initially generated electron – hole pairs rapidly recombine or become trapped at defect centers, swiftly saturating their contribution to photoconductivity.

Subsequently, the photoionization of oxygen vacancies becomes the dominant source of excess electrons, further increasing the carrier concentration. Upon illumination, oxygen vacancies become ionized, forming donor levels according to the reaction.

$$V_o \rightarrow V_o^{2+} + 2e \tag{15}$$

Given a specific photon flux, and assuming an ionization rate constant C_i, then

$$\frac{dN_d(t)}{dt} = C_i[N_{V0} - N_d(t)] \tag{16}$$

Here, N_d denotes the density of ionized donor states, and C_i represents the ionization rate constant. The corresponding solution is

$$N_d(t) = N_{V0}(1 - e^{-C_i t} \tag{17}$$

The contribution of ionized donor concentrations must be considered when oxygen vacancies increase due to vacuum annealing. Accordingly, the conductivity expression in Eq. (13) was modified as follows:

$$\sigma = \sigma_d + \sigma_{po} \frac{1}{1 + A\left(1 - \mathrm{e}^{-\frac{t}{\tau_d}}\right)} + N_{V0}(1 - e^{-C_i t}) e\mu \tag{18}$$

From Eq. (5),

$$\mathrm{e}\mu N_{V_0} = \frac{\sigma_d - G\tau_o e\mu}{\alpha \tau_0} \tag{19}$$

Then, Eq. (18) becomes.

$$\sigma = \sigma_{d0}\left(1 + \frac{\alpha N_{Vo}}{G}\right) + \frac{\sigma_{po}}{1 + A\left(1 - \mathrm{e}^{-\frac{t}{\tau_d}}\right)} + \frac{\sigma_d - G\tau_o e\mu}{\alpha \tau_0}(1 - e^{-C_i t}) \tag{20}$$

Since the dark conductivity depends on the oxygen vacancy concentration, N_{Vo}, as described in Eq. (5), the values of N_{Vo} were calculated, as presented in Table 2. The calculation was performed using Eq. (5), assuming $\sigma_{d0} = 1.0 \times 10^{-12}$ S/cm, and $\alpha/G = 1.0 \times 10^{-10}$, which provided the best fit with minimal error.

Equation (20) is the whole equation used to present the dark and photoconductivities. As just varying N_{Vo}, the conductivities were calculated. The conductivities for $N_{Vo} = 1.0 \times 10^{15}\mathrm{cm}^{-3}$, $4.0 \times 10^{18}\mathrm{cm}^{-3}$ and $5.0 \times 10^{19}\mathrm{cm}^{-3}$ are specified in Figure 6(a–c), respectively. A, τ_d, and C_i are fitting parameters and were not varied. $G\tau_o e\mu$ is σ_{d0}, and assuming $1 \times 10^{-12} S$ / cm which gave the best fit for the extraction of N_{Vo}. The initial sharp increase in conductivity upon light illumination, followed by a gradual decrease in photoconductivity over time, aligns well with the photo response behavior delineated in Figure 2(b). For the larger oxygen vacancies, a slow increase in the photoconductivity is observed, aligning with the measured results shown in Figure 3(b).

These results demonstrate that the photoconductive properties of a-IGZO films are significantly influenced by the density of oxygen vacancies, which plays a crucial role in determining dark and photoconductivity by acting as donor states that contribute free electrons to the conduction band. The oxygen vacancy concentration can be

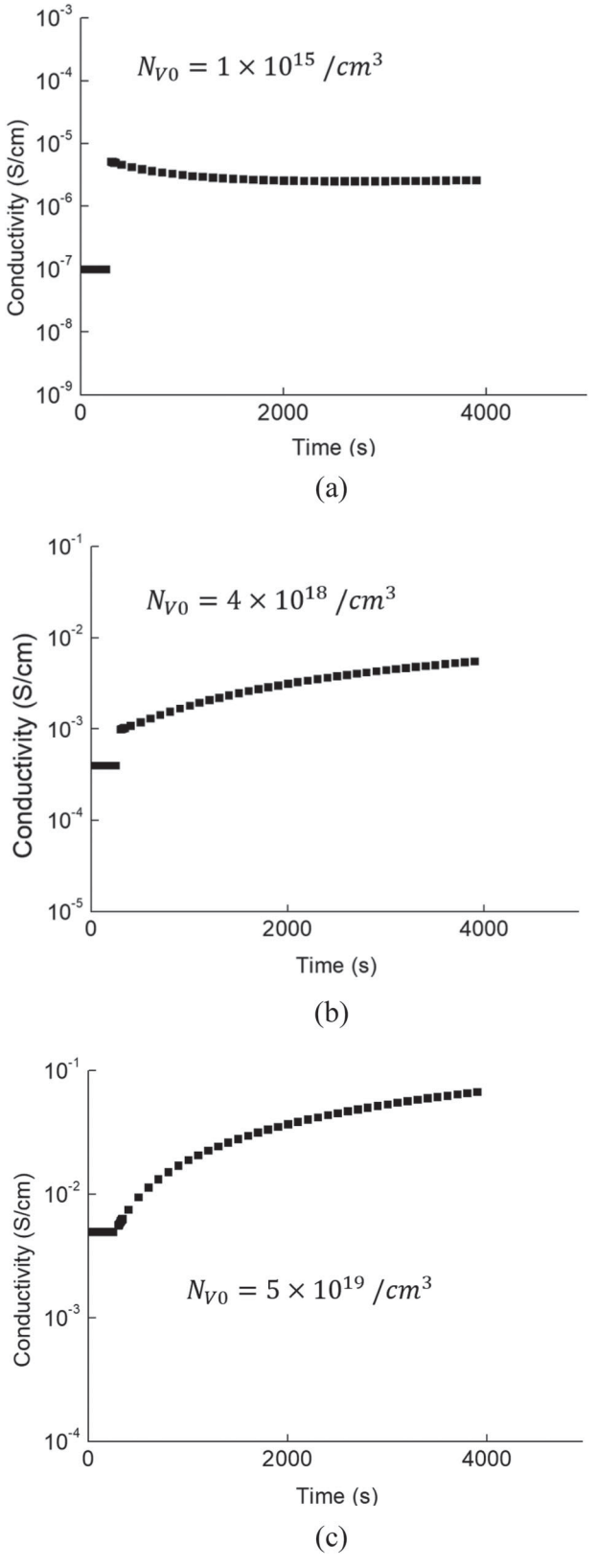

Figure 6. Calculated conductivity just varying the oxygen vacancy concentrations (a) for $N_{Vo} = 1.0 \times 10^{15} cm^{-3}$, (b) for $4.0 \times 10^{18} cm^{-3}$ and (*c*)*for*$5.0 \times 10^{19} cm^{-3}$.

precisely controlled through the annealing temperature, with higher temperatures typically increasing vacancy density. This increase enhances the self-doping effect, where ionized oxygen vacancies provide a steady supply of free charge carriers, thereby improving dark and photoconductivity. The annealing process is thus a powerful method for tuning the photoconductive response of a-IGZO films, which is vital for applications in devices like displays and sensors that rely on controlled electrical conductivity under varying light conditions.

4. Conclusions

We investigated the photo-response behavior of a-IGZO films and identified three distinct photoconductivity types, categorized by oxygen vacancy density: low (Type I), intermediate (Type II), and high (Type III). The results indicate that the photoconductive properties of the films are strongly influenced by the concentration of oxygen vacancies, which can be precisely controlled through annealing processes. Type I, characterized by low vacancy density, exhibits rapid recombination of electron–hole pairs, while Type II and Type III yield progressively slower recombination and more persistent photoconductivity, reflecting the increasing impact of ionized oxygen vacancies as donor states. These findings provide valuable insights for optimizing a-IGZO films for various device applications, such as displays and sensors, where controlling photoconductivity is crucial. Furthermore, the observed photoconductive behavior under light illumination serves as an effective measure of the film's quality, highlighting the value of oxygen vacancy engineering in customizing the electronic properties of a-IGZO for specific technological uses.

Acknowledgments

This paper was supported by the Korea Institute for Advancement of Technology (KIAT) grant, funded by the Korean government (Ministry of Trade, Industry and Energy [MOTIE]) (RS-2025-02263458, HRD Program for Industrial Innovation), and the National Research Foundation of Korea Grant, funded by the Korean Government (NRF-2022K1A3A1A20015124).

Disclosure statement

No potential conflict of interest was reported by the authors.

Funding

This work was supported by National Research Foundation of Korea: [Grant Number 2021RIS-004].

Notes on contributors

Seung-Jae Moon received his Bachelor's and Master's degrees in Digital Display Engineering from Hoseo University in Asan, Chungnam, South Korea in 2014 and 2017, respectively. In 2020, he obtained his Ph.D. in Microelectronics based on inkjet printing technology from both Hoseo University in Asan, South Korea and Rennes 1 University in France. From 2020 to 2022, he worked as a postdoctoral researcher at CNRS, France, focusing on the evaluation of new organic semiconductor materials for TFT structures used in sensors and bio-based raw materials for electronic products. Currently, he is a postdoctoral researcher jointly affiliated with Hoseo University in Asan, Chungnam, South Korea, and Ulsan National Institute of Science and Technology (UNIST) in Ulsan, South Korea. His research areas include inkjet printing-based organic/inorganic TFTs, displays, integrated circuits, and sensors.

Ju-Yeon Kim received his B.S and M.S in Digital Display Engineering from Hoseo University in Asan, Chungnam, South Korea in 2013 and 2015, respectively. From 2015 to 2017, he worked as process engineer at Invenia Corporation. Since 2017, he has been dedicated mainly to Nand Flash Memory application at Lam Research Korea.

Junghwan Kim received his B.S. (2012) in electrical engineering and computer science at Ajou University, Korea and his M.S. (2014) and Ph.D. (2016) in innovative engineered materials at Tokyo Institute of Technology, Japan. His main research interests include exploring new functional materials and developing electronic devices. Before joining the Ulsan National Institute of Science & Technology (UNIST), he was an assistant professor at Tokyo Institute of Technology since 2016. He has been dedicated mainly to metal oxide and halide materials and related devices, such as thin-film transistors and light-emitting diodes, over the last decade. By joining UNIST, he plans to apply his background to future electronics, such as AI devices and next-generation memory applications.

Byung Seong Bae received his B.S. Atomic Nuclear Engineering degree from Seoul National University, Seoul, South Korea, in 1980, and his M.S. and Ph.D. Applied Physics degrees from Korea Advanced Science and Technology, Seoul, South Korea, in 1986 and 1991, respectively. From 1991 to 1998, he worked at Samsung Electronics, particularly on the development of an amorphous and polysilicon TFT backplane with an integrated driver. From 1999 to 2003, he set up a high-temperature polysilicon TFT micro display factory and developed a micro display for projection at ILJIN Display. Since 2006, he has been a professor at the-Hoseo University in Asan, South Korea. His current research areas include TFTs, sensors, displays, and integrated circuits of TFTs.

References

[1] B.J. Park, S.W. Chung, M.J. Kim, H.J. Lee, J.H. Bae, S.C. Kang, and J.K. Jeong, IEEE Electron Device Lett **44**, 1857 (2023).

[2] K. Nomura, H. Ohta, A. Takagi, T. Kamiya, M. Hirano, and H. Hosono, Nature **432**, 488 (2004).

[3] B. Lu, F. Zhuge, Y. Zhao, Y–J Zeng, L. Zhang, J. Huang, Z. Ye, and J. Lu, Curr. Opin. Solid State Mater. Sci **27**, 101092 (2023).

[4] J. Yoo, J.-H. Hong, H. Kim, D. Kim, C. Lee, M. Kim, C. Byun, and B. Choi, Mat. Sci. Semicon. Proc **157**, 107299 (2023).

[5] H. Oh, S.-M. Yoon, M.K. Ryu, C.-S. Hwang, S. Yang, and S.-H.K. Park, Appl. Phys. Lett **97**, 183502 (2010).

[6] Y. Yang, H. Ning, D. Luo, Z. Xu, Z. Fang, W. Xu, Z. Zhang, B. Jiang, R. Yao, and J. Peng, Surfaces and Interfaces **44**, 103704 (2024).

[7] M.D.H. Chowdhury, P. Migliorato, and J. Jang, Appl. Phys. Lett **97**, 173506 (2010).

[8] H.-S. Kim, S.H. Jeon, J.S. Park, T.S. Kim, K.S. Son, J.-B. Seon, S.-J. Seo, S.-J. Kim, E. Lee, J.G. Chung, H. Lee, S. Han, M. Ryu, S.Y. Lee, and K. Kim, Sci. Rep **3**, 1459 (2013).

[9] T. Kamiya, K. Nomura, and H. Hosono, Phys, Status Solidi A **207**, 1698 (2010).

[10] J.S. Park, W.-J. Maeng, H.-S. Kim, and J.-S. Park, Thin Solid Films **520**, 1679 (2012).

[11] S.K. Park, M. Ryu, S. Yang, S.M. Yoon, and C. Hwang, J. Inf. Disp **11**, 113 (2010).

[12] D.-Y. Cho, J. Song, C.S. Hwang, W.S. Choi, T.W. Noh, J.-Y. Kim, H.-G. Lee, B.-G. Park, S.-Y. Cho, S.-J. Oh, J.H. Jeong, J.K. Jeong, and Y.-G. Mo, Thin Solid Films **518**, 1079 (2009).

[13] Y. Zhang, X. Wang, S. Zhang, C. Wang, and M. Zhang, IEEE Open Journal on Immersive Displays **1**, 187 (2024).

[14] T. Sakai, H. Seo, S. Aihara, M. Kubota, N. Egami, D. Wang, and M. Furuta, Jpn. J. Appl. Phys **51**, 010202 (2011).

[15] H. Kitakado, and S. Katoh, Jpn. J. Appl. Phys **51**, 03CB02 (2012).

[16] J. Luo, A.U. Adler, T.O. Mason, D.B. Buchholz, R.P.H. Chang, and M. Grayson, J. Appl. Phys **113**, 153709 (2013).

[17] T. Kamiya, K. Nomura, and H. Hosono, Sci. Technol. Adv. Mater **11**, 044305 (2010).

[18] S.-H. Lim, D.-G. Mah, and W.-J. Cho, Nanomaterials **14**, 1252 (2024).

[19] L. Liang, H. Zhang, T. Li, W. Li, J. Gao, H. Zhang, M. Guo, S. Gao, Z. He, F. Liu, C. Ning, H. Cao, G. Yuan, and C. Liu, Adv, Sci **10**, 2300373 (2023).

[20] B. Ryu, H.-K. Noh, E–A Choi, and K.J. Chang, Appl. Phys. Lett **97**, 022108 (2010).

[21] W.-J. Lee, E.-A. Choi, J. Bang, B. Ryu, and K.J. Chang, Appl. Phys. Lett **93**, 111901 (2008).

[22] A. Takagi, K. Nomura, H. Ohta, H. Yanagi, T. Kamiya, M. Hirano, and H. Hosono, Thin Solid Films **486**, 38 (2005).

[23] Y.-M. Kim, K.-S. Jeong, H.-J. Yun, S.-D. Yang, S.-Y. Lee, H.-D. Lee, and G.-W. Lee, Jpn. J. Appl. Phys **51**, 09M–F10 (2012).
[24] Z. Lin, L. Kang, J. Zhao, Y. Yin, Z. Wang, J. Yu, Y. Li, G. Yi, A. Nathan, X. Li, Y. Wu, J. Xu, and M. Si, IEEE Trans. Electron Dev **71**, 3002 (2024).
[25] Y. Shi, M. Tsuji, H. Cho, S. Ueda, J. Kim, and H. Hosono, ACS Nano **18**, 9736 (2024).
[26] B.K. Yap, Z. Zhang, G.S.H. Thien, K.-Y. Chan, and C.Y. Tan, Appl. Surf. Sci. Adv **16**, 100423 (2023).
[27] C.G. Van de Walle, Phys. Rev. Lett **85**, 1012 (2000).
[28] A.K. Singh, A. Janotti, M. Scheffler, and C.G. Van de Walle, Phys. Rev. Lett **101**, 055502 (2008).
[29] K.H. Ji, J.-I. Kim, H.Y. Jung, S.Y. Park, R. Choi, U.K. Kim, C.S. Hwang, D. Lee, H. Hwang, and J.K. Jeong, Appl. Phys. Lett **98**, 103509 (2011).
[30] D. Redfield, and R.H. Bube, Philos, Mag. B **74**, 309 (1996).
[31] B.-W. Chen, T.-C. Chang, Y.-J. Hung, T.-Y. Hsieh, M.-Y. Tsai, P.-Y. Liao, W.-W. Tsai, W.-J. Chiang, and J.-Y. Yan, Thin Solid Films **572**, 33 (2014).
[32] J.K. Jeong, H.W. Yang, J.H. Jeong, Y.-G. Mo, and H.D. Kim, Appl. Phys. Lett **93**, 123508 (2008).
[33] T.-C. Chen, T.-C. Chang, T.-Y. Hsieh, C.-T. Tsai, S.-C. Chen, C.-S. Lin, M.-C. Hung, C.-H. Tu, J.-J. Chang, and P.-L. Chen, Appl. Phys. Lett **97**, 192103 (2010).
[34] J.T. Yuh, and B.S. Bae, Electron. Mater. Lett **6**, 221 (2010).
[35] K.M. Yu, J.T. Yuh, S.H.K. Park, M.K. Ryu, E.J. Yun, and B.S. Bae, Jpn. J. Appl. Phys **52**, 10M–A12 (2013).
[36] N. Choi, M.J. Kim, H. Hong, D.Y. Shin, J. Go, T.G. Weldemhret, K. Jeong, and K.-B. Chung, IEEE Trans. Electron Dev **71**, 5393 (2024).
[37] P. Wang, Y. Lan, C. Huan, J. Luo, W. Cai, J. Fan, X. He, Z. Huang, L. Zhu, Q. Ke, G. Zhang, and S. Lin, Mater Sci Eng R: Rep **156**, 100759 (2023).
[38] J.H. Kim, U.K. Kim, Y.J. Chung, and C.S. Hwang, Appl. Phys. Lett **98**, 232102 (2011).
[39] T. Shimizu, Jpn, J. Appl. Phys **43**, 3257 (2004).
[40] D.L. Staebler, and C.R. Wronski, Appl. Phys. Lett **31**, 292 (1977).
[41] D.L. Staebler, and C.R. Wronski, J. Appl. Phys **51**, 3262 (1980).
[42] M. Mativenga, F. Haque, M.M. Billah, and J.G. Um, Sci, Rep **11**, 14618 (2021).